Asian Journal of Chemistry; Vol. 26, No. 7 (2014), 2141-2146

ASIAN JOURNAL OF CHEMISTRY

http://dx.doi.org/10.14233/ajchem.2014.16534

Synthesis and Characterization of $FeO/Ni_{0.5}Mn_{0.5}Fe_2O_4$ Nano-Composite

N.M. DERAZ[1,*] and OMAR H. ABD-ELKADER[2,3]

[1]Physical Chemistry Department, Laboratory of Surface Chemistry and Catalysis, National Research Center, Dokki, Cairo, Egypt
[2]Zoology Department, College of Science, King Saud University, Riyadh 11451, Kingdom of Saudi Arabia
[3]Electron Microscope and Thin Films Department, National Research Center, El- Behooth Street, 12622, Giza, Egypt

*Corresponding author: E-mail: nmderaz@yahoo.com

Received: 16 October 2013; *Accepted*: 20 November 2013; *Published online*: 22 March 2014; AJC-14979

$FeO/Ni_{0.5}Mn_{0.5}Fe_2O_4$ nano-composite was prepared using glycine assisted combustion method. The structure, morphology, chemical composition and magnetization of the as prepared composite was studied using X-ray diffraction, infrared spectroscopy, scanning electron micrographs, energy dispersive X-ray and a vibrating sample magnetometer. The structural parameters such as crystallite size, lattice constant, unit cell volume and theoretical density of the constituents of composite (FeO and $Ni_{0.5}Mn_{0.5}Fe_2O_4$) have been determined. X-ray diffraction and infrared measurements confirm formation of both $Ni_{0.5}Mn_{0.5}Fe_2O_4$ and FeO phases. SEM technique was used to investigate the morphology characteristics of the investigated solid. It was found that the as synthesized composite consisted of polyhedron, spongy, homogeneous and fragile materials. Also, energy dispersive X-ray technique showed the concentrations of O, Ni, Fe and Mn species involved in the prepared composite specimen from the uppermost surface to the bulk layers indicating to the elements gradient. The saturation magnetization (M_s), remanence magnetization (M_r) and coercivity (H_c) of the as synthesized composite were 71 emu/g, 24 emu/g and 272 Oe, respectively.

Keywords: XRD, IR, SEM, EDX, $Ni_{0.5}Mn_{0.5}Fe_2O_4$, FeO.

INTRODUCTION

It is an interesting question that why all this attention to the preparation and characterization of different types of ferrites? Here we find many reasons, including high resistivity, applicability at higher frequency, lower price, greater heat resistance and higher corrosion resistance. It was found that the resistivity of ferrites varies from 10^2 to 10^{10} ohm-cm which is about 15 orders of magnitude higher than that of iron[1]. Ferrites have many application areas at higher frequency depending upon the high resistivity. As a result of technological progress increased the demand for soft magnetic materials day after day especially ferrite due to their unique physical and chemical properties such as their high thermodynamic stability, electrical resistivity, electrolytic activity, low cost, easy to synthesize and resistance to corrosion[2,3]. These properties are dependent upon different parameters such as composition, preparation route, dopant, time and temperature of preparation, precursor's history, grain size and distribution of reacting cations[4,5].

Inverse spinel nickel ferrite was prepared by combustion method using glycine as fuel[6]. Effect of magnesia doping on different properties of nickel ferrite has been studied. XRD measurements showed formation of single nickel ferrite phase with spongy and fragile network structure. The increase in magnesia concentration resulted in a decrease in the saturation magnetization, average crystallite size, lattice constant, unit cell volume, X-ray density, ionic radii, the distance between the magnetic ions and bond lengths on tetrahedral sites and octahedral sites of the as prepared ferrite[6].

Nano-sized $MnFe_2O_4$ system has been prepared using glycine - assisted combustion technique[7]. The effects of the ratio between metal nitrate and glycine as fuel on structural, morphological, surface, magnetic and catalytic activity towards conversion of cyclohexene have been investigated. Single-domain $MnFe_2O_4$ nano-particles was formed when the ratio of glycine to metal nitrate was 2.67. The increase in the amount of fuel led to an increase in magnetization, coercivity and activity of manganese ferrite. All solids investigated behaved as dehydrogenation catalysts. Maximum magnetization (68.58 emu/g) and coercivity (62.57 Oe) values of the investigated ferrite were determined at the ratio of 2.67. Opposite behavior was observed in the case of The BET surface area of the investigated solids[7].

Several investigations were reported to prepare mixed nickel-manganese ferrites using different preparation methods[8-13]. Some authors pointed that the addition of a certain amounts of Ni species to manganese ferrite at elevated temperatures resulted in a decrease in the conversion of Mn^{2+} to Mn^{3+} ions

at the surface layer with subsequent an increase in the stability of the Ni-Mn ferrite[11,12]. In other words, the thermal stability of the mixed ferrite is greater than that of single ferrite. Other investigators claimed that the increase in the content of Mn species involved in the mixed ferrite led to formation of iron oxide as a secondary phase[13]. However, the change in the molar ratio of the reacting species led to a significant modification in different properties of the as prepared mixed ferrites[8-13].

This paper aims to synthesize the nano-crystalline $FeO/Ni_{0.5}Mn_{0.5}Fe_2O_4$ nano-composite by combustion route depending upon glycine as fuel. The elemental analysis and different properties such as structural, spectroscopic, morphological and magnetic characteristics of nano- composite have been investigated. XRD, IR, SEM, EDX and vibrating sample magnetometer techniques were used for characterization of this system.

EXPERIMENTAL

Preparation procedure: Mixture of calculated proportions of nickel, manganese and iron nitrates were used to prepare $FeO/Ni_{0.5}Mn_{0.5}Fe_2O_4$ composite specimen. The mixture of different precursors was concentrated in a porcelain crucible on a hot plate at 400 °C for 5 min. The crystal water was gradually vaporized during heating and when a crucible temperature was reached, a great deal of foams produced and spark appeared at one corner which spread through the mass, yielding a brown voluminous and fluffy product in the container. In this study, the ratio of the H_2NCH_2COOH : $Ni(NO_3)_2{\cdot}4H_2O$: $Mn(NO_3)_2{\cdot}6H_2O$:$Fe(NO_3)_3.9H_2O$ were 4:0.5:0.5:2, respectively. The chemicals employed in the present work were of analytical grade supplied by Prolabo Company.

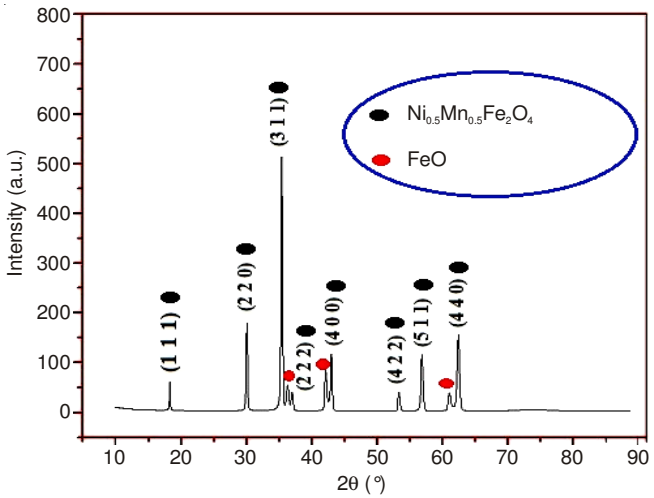

Fig. 1. XRD pattern for the as prepared sample

Characterization technique: An X-ray measurement of various mixed solids was carried out using a BRUKER D8 advance diffractometer (Germany). The patterns were run with CuK_α radiation at 40 kV and 40 mA with scanning speed in 2θ of 2° min^{-1}.

The crystallite size of FeO and $Ni_{0.5}Mn_{0.5}Fe_2O_4$ present in the investigated solids was based on X-ray diffraction line broadening and calculated by using Scherrer equation[14].

$$d = \frac{B\lambda}{\beta\cos\theta} \quad (1)$$

where d is the average crystallite size of the phase under investigation, B is the Scherrer constant (0.89), λ is the wave length of X-ray beam used, β is the full-width half maximum (FWHM) of diffraction and θ is the Bragg's angle.

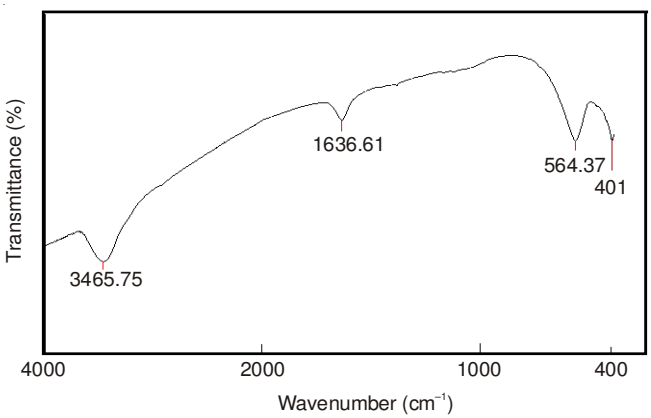

Fig. 2. IR spectra of the as prepared sample

An infrared transmission spectrum of various solids was determined using Perkin-Elmer Spectrophotometer (type 1430). The IR spectra were determined from 900 to 300 cm^{-1}. Two mg of each solid sample were mixed with 200 mg of vacuum-dried IR-grade KBr. The mixture was dispersed by grinding for 3 min in a vibratory ball mill and placed in a steel die 13 mm in diameter and subjected to a pressure of 12 tones. The sample disks were placed in the holder of the double grating IR spectrometer.

Scanning electron micrographs (SEM) was recorded on JEOL JAX-840A electron micro-analyzer. The sample was dispersed in ethanol and then treated ultrasonically in order to disperse individual particles over gold grids.

Energy dispersive X-ray analysis (EDX) was carried out on Hitachi S-800 electron microscope with an attached kevex Delta system. The parameters were as follows: accelerating voltage 15 kV, accumulation time 100s, window width 8 μm. The surface molar composition was determined by the Asa method, Zaf-correction, Gaussian approximation.

The magnetic properties of the investigated solids were measured at room temperature using a vibrating sample magnetometer (VSM; 9600-1 LDJ, USA) in a maximum applied field of 15 kOe. From the obtained hysteresis loops, the saturation magnetization (M_s), remanence magnetization (M_r) and coercivity (H_c) were determined.

RESULTS AND DISCUSSION

Structural properties: XRD pattern of the as synthesized solid was illustriated in Fig. 1. In fact, the diffraction pattern of the $MnFe_2O_4$ phase (JCPDS: 75-0034) is similar to the $NiFe_2O_4$ phase (JCPDS: 86-2267). Fig. 1 shows the following planes: (1 1 1), (2 2 0), (311), (2 2 2), (4 0 0), (4 2 2), (5 1 1) and (4 4 0), respectively. These planes are consistent with all planes related to $MnFe_2O_4$ and $NiFe_2O_4$ phases pointed to a significant shift in the diffraction lines for the investigated solid

indicating formation of $Ni_{0.5}Mn_{0.5}Fe_2O_4$ spinel (major phase) with the *Fd3m* space group. The average crystallite size of $Ni_{0.5}Mn_{0.5}Fe_2O_4$ phase was estimated to be about 55 nm. However, it was observed formation of FeO (minor phase) as a second material[13]. The crystallite size of cubic FeO (wustite, syn) is 20 nm with the *Fm3m* space group. These findings suggest the formation of FeO/$Ni_{0.5}Mn_{0.5}Fe_2O_4$ nano-composite.

Depending on X-ray data, we can estimate the different structural parameters of $Ni_{0.5}Mn_{0.5}Fe_2O_4$ such as the distance between the magnetic ions (L_A and L_B), ionic radii (r_A, r_B) and bond lengths (A-O and B-O) on tetrahedral (A) sites and octahedral (B) sites. The estimated values of L_A, L_B , r_A, r_B, A-O and B-O of $Ni_{0.5}Mn_{0.5}Fe_2O_4$ particles are 0.3514, 0.2941, 0.0548, 0.0668, 0.1918 and 0.2128 nm, respectively.

Functional group analysis: An IR spectrum of the as prepared composite, in the range of 4000-400 cm^{-1}, was determined as shown in Fig. 2. It can see from this figure that the as prepared composite has two principle metal-oxygen bands referred to the spinel structure. The first band ν_1 locates at 564.37 cm^{-1}. This band corresponds to intrinsic stretching vibrations of metal at the tetrahedral site (Fe ↔ O). The second band sited at 401 cm^{-1}. This band related to octahedral-metal stretching (Ni ↔ O and Mn ↔ O). In addition, two broad bands at 3465.75 cm^{-1} and 1636.61 cm^{-1} are related to the stretching modes and H-O-H bending vibration of the free or absorbed water[15].

SEM investigation: Fig. 3A-D refers the scanning electron micrographs (SEM) of the as synthesized solid on various points with different magnifications. From this figure, we can determine the morphology of composite studied. The as synthesized sample consisted entirely of polyhedron, spongy and fragile materials. However, various voids and pores were observed in the as prepared composite.

EDX measurements: Investigation of the homogeneity, elements gradient and chemical composition of the presented composite can be achieved using Energy dispersive X-ray (EDX) technique with different voltages and also different points on the surface of sample. Figs. 4 and 5 show the EDX spectra at different points on the surface of sample and different applied voltages, respectively.

Homogeneity of elements: The concentrations of various elements (O, Mn, Fe and Ni) involved in the investigated solid at 20 keV over different points on the sample surface are shown in Table-1. These concentrations are very close to each other. This confirms the homogeneity of the as prepared system.

Element gradient: The concentrations of O, Mn, Fe and Ni species from the uppermost surface to the bulk layers of the sample of Ni-Zn ferrite were determined using EDX technique at 10, 15 and 20 keV as shown in Table-2. Table-2 showed that the concentrations of Mn and O species for the as prepared sample are close to each other at different applied voltages. The concentration of Fe species increases as the applied voltage increases. The opposite behavior was observed in the case of Ni species. In addition, the concentrations of both Mn and Ni species are close to each other at different points and also with various applied voltages. This suggested that equimolar ratio of both Mn and Ni species were reacted with a certain amount of iron species yielding $Ni_{0.5}Mn_{0.5}Fe_2O_4$

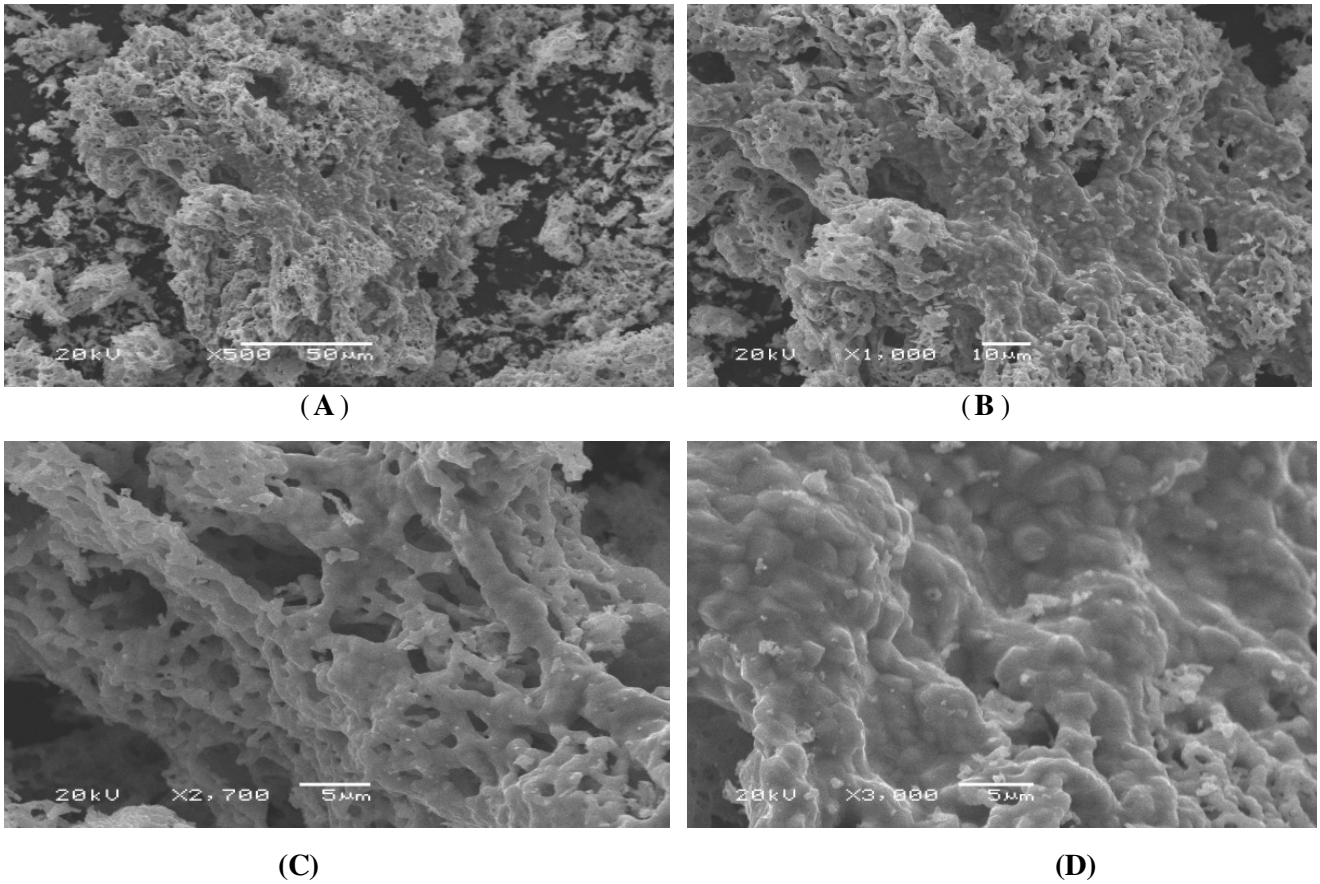

(A) (B)

(C) (D)

Fig. 3. SEM images for as prepared sample on various points with different magnifications

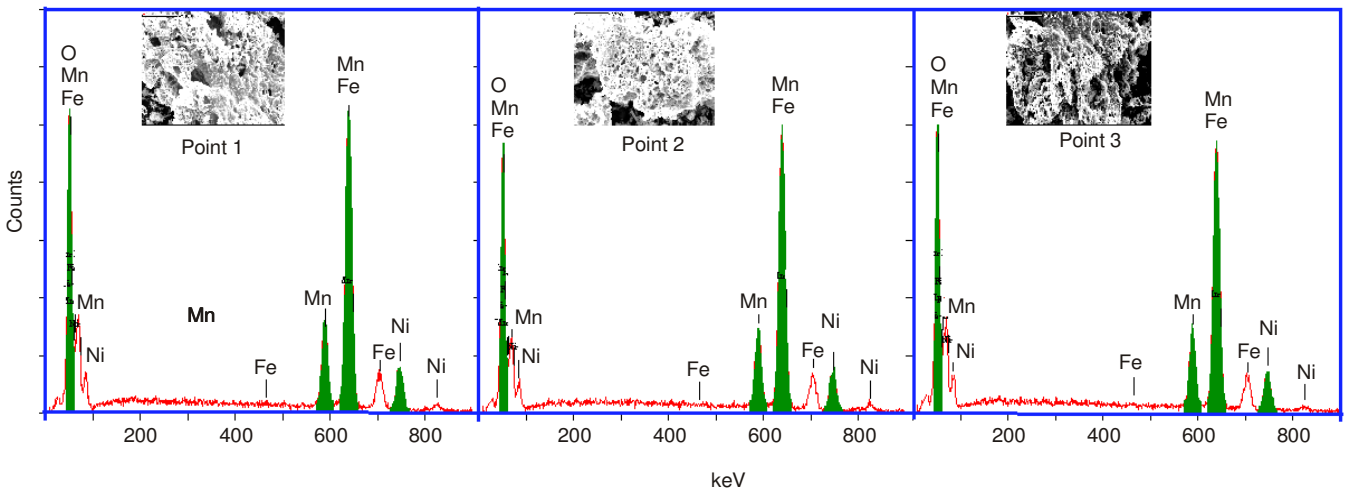

Fig. 4. EDX patterns of the as prepared sample with different points

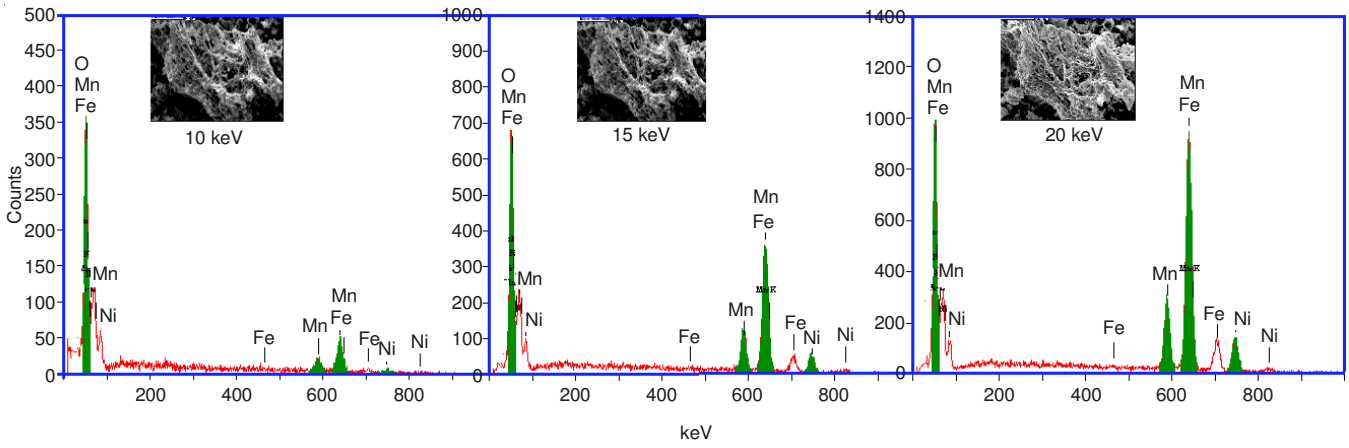

Fig. 5. EDX patterns of the as prepared sample at 20 keV with different voltages

TABLE-1
MASS ABUNDANCE OF ELEMENTS MEASURED AT 20 KEV AT DIFFERENT POINTS OVER THE AS PREPARED SAMPLE

Sample	Elements	Point 1	Point 2	Point 3
Composite	O	22.18	22.18	22.18
	Mn	12.07	12.24	12.39
	Fe	53.27	53.44	52.13
	Ni	12.49	12.13	12.30

TABLE-2
MASS ABUNDANCE OF ELEMENTS MEASURED AT DIFFERENT APPLIED VOLTAGES ON THE ONE POINT OVER THE AS PREPARED SAMPLE

Sample	Elements	10 eV	15 eV	20 eV
Composite	O	22.17	22.19	22.19
	Mn	12.07	12.33	12.13
	Fe	52.29	53.74	54.07
	Ni	13.47	11.74	11.61

solid. However, the concentration of Fe species is higher than the Fe content that must be present in the stoichiometric percentage indicating to un-reacted amount of iron. Indeed, XRD measurements showed that FeO was observed as a second phase.

Magnetic properties: The magnetic properties of the as-prepared powders were determined by measuring the magnetic hysteresis loop at room temperature as shown in Fig. 6. The values of M_s, M_r and H_c for the as prepared composite were 71 emu/g, 24 emu/g and 272 Oe, respectively. The comparison between these values and that for both $MnFe_2O_4$ and $NiFe_2O_4$ showed that the magnetic parameter of the as prepared composite are higher than that of both nickel and manganese ferrites.

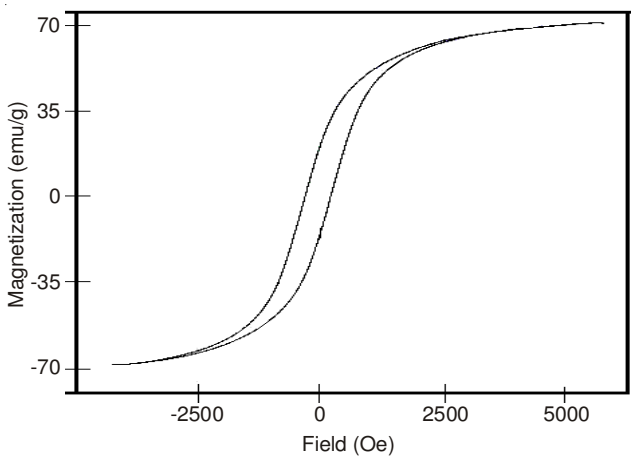

Fig. 6. Magnetic hysteresis curves measured at a room temperature for the as prepared sample

Our research group used the glycine-assisted combustion method for preparation of both $NiFe_2O_4$ and $MnFe_2O_4$ nano-particles[6,7]. This method has different advantages. The important characteristic for this method is the uniform heat distribution through the whole mass of the as synthesized sample. In other words, the reaction in the combustion route proceeds predominantly from the periphery of the reaction bulk to its centre. This process allows formation of individual oxide phase nuclei that may be distributed in the sample volume. These nuclei have high reactivity and homogeneous distribution with subsequent elimination of diffusion barriers which prevents the process of phase formation.

In fact, dissolution of trivalent cations into NiO or MnO with appearance of ferric cations in tetrahedral site is an embryonic element or nucleus for spinel formation[16]. The mechanism of $Ni_{0.5}Mn_{0.5}Fe_2O_4$ formation depends on the diffusion of Mn^{2+}, Ni^{2+} and Fe^{3+} through early rigid ferrite film[6,7]. This diffusion was depended on the difference in the ionic radii of the reacting cations. In addition, the diffusion of the reacting cations led to create chemically vacancies. The diffusing ions might be Fe^{2+} including Fe^{3+} depending on the detecting Fe^{2+} in the interface[17]. Some authors indicate that Fe_2O_3 decomposes to $2Fe^{2+}$ and oxygen gas at Fe_2O_3-interface[18]. Moreover, oxygen moves through the reacted area to be added to the NiO and MnO interfaces in order to form spinel by reacting with Fe^{2+} and NiO and MnO:

At Fe_2O_3 interface:

$$3Fe_2O_3 + Ni^{2+} + Mn^{2+} \rightarrow 2Ni_{0.5}Mn_{0.5}Fe_2O_4 + 2Fe^{2+} + 0.5O_2 \quad (2)$$

At NiO and MnO interfaces:

$$2Fe^{2+} + 1.5NiO + 1.5\ MnO + 0.5O_2 \rightarrow Ni_{0.5}Mn_{0.5}Fe_2O_4 + Ni^{2+} + Mn^{2+} \quad (3)$$

The comparison between the structural parameters (especially a, V and D_x) for $Ni_{0.5}Mn_{0.5}Fe_2O_4$ system in this study and our previous investigations about $NiFe_2O_4$ and $MnFe_2O_4$ is very important. It can be seen that the values of lattice constant and unit cell volume of $Ni_{0.5}Mn_{0.5}Fe_2O_4$ are in the range between that for both $NiFe_2O_4$ and $MnFe_2O_4$ systems. These observations were confirmed by the presented shift in the X-ray diffraction lines of $Ni_{0.5}Mn_{0.5}Fe_2O_4$ system comparing with that of both nickel and zinc ferrites. The lattice constant of $Ni_{0.5}Mn_{0.5}Fe_2O_4$ was found to be 0.84 nm, which is in agreement with the reported values of 0.8340 nm and 0.8461 for $NiFe_2O_4$ and $MnFe_2O_4$, respectively[6,7]. However, IR spectra confirm the formation of $Ni_{0.5}Mn_{0.5}Fe_2O_4$ spinel. The calculated values of the lattice constant, unit cell volume and X- ray density of both $Ni_{0.5}Mn_{0.5}Fe_2O_4$ and FeO are listed in Table- 3. This table displays that the lattice constant of $Ni_{0.5}Mn_{0.5}Fe_2O_4$ is greater than that of FeO. This confirms that the grain size of FeO is lower than that of $Ni_{0.5}Mn_{0.5}Fe_2O_4$ as discussed by the XRD.

TABLE-3
SOME STRUCTURAL PARAMETERS FOR THE CONSTITUENTS OF THE AS PREPARED COMPOSITE

Parameters	$Ni_{0.5}Mn_{0.5}Fe_2O_4$	FeO
a	0.8400	0.4284
V	0.5927	0.7863
D_x	5.8621	5.9690

Energy dispersive X-ray measurements showed that the surface concentrations of Ni species for the as prepared sample increase and that of Zn decrease as the applied voltage increases with fixed the surface concentrations of both O and Fe species. This refers that MnO was dissolved in both NiO and Fe_2O_3 solids forming $Ni_{0.5}Mn_{0.5}Fe_2O_4$ solid. SEM measurements showed that the glycine- assisted combustion route led to formation of fragile, spongy and homogeneous $Ni_{0.5}Mn_{0.5}Fe_2O_4$ solid.

In fact, the common iron oxides group consisted of hematite, maghemite and magnetite. One form of this group is wustite (FeO) having a rock-salt structure with Fe and O forming non-stoichiometric Fe_xO (x = 0.83-0.96) and Fe vacancies in an ordered distribution[19]. FeO is not chemically stable due to its decomposition into α- Fe_2O_3 and inverse spinel Fe_3O_4[20]. This chemical reactivity displays difficult in the preparation process of this oxide from the high-temperature solution-phase decomposition of iron salt[20]. But, this study shows formation of FeO nano-particles during preparation of $Ni_{0.5}Mn_{0.5}Fe_2O_4$. This indicates that Ni-Mn ferrite is stabilizer for preparation of FeO. In other words, the presence of $Ni_{0.5}Mn_{0.5}Fe_2O_4$ resulted in an increase in the chemical stability of FeO nan-particles.

The saturation magnetization of the as synthesized sample is larger than the value obtained for Ni and Mn ferrites prepared by the same method in our previous investigations[6,7]. This can be attributed to larger magnetic moments of Mn ions ($5\mu_B$) substituted with Ni ions having smaller magnetic moments of ($2.83\mu_B$) at the octahedral site, however, presence of FeO as a second phase[10,21]. In other words, these enhanced magnetic properties for the composite ferrite can be attributed to the exchange-coupling interaction in the composite. Similar results were observed in the case of $Zn_{0.5}Mn_{0.5}Fe_2O_4$ sample[22].

Conclusion

FeO/$Ni_{0.5}Mn_{0.5}Fe_2O_4$ nano-composite was prepared by using glycine- assisted combustion route depending upon the solid state reaction between NiO, MnO and Fe_2O_3. The lattice constant, unit cell volume, X-ray density, the distance between the magnetic ions, ionic radii and bond lengths on tetrahedral and octahedral sites of the constituents involved in the as prepared nano-composite have been determined. This method resulted in polyhedron, spongy and homogeneous solid with

formation of both spinel $Ni_{0.5}Mn_{0.5}Fe_2O_4$ and FeO phases. These findings were confirmed by depending upon XRD, IR, SEM and EDX techniques. The magnetic properties of the as prepared composite are best of that for manganese and nickel ferrites.

ACKNOWLEDGEMENTS

This project was supported by King Saud University, Deanship of Scientific Research, College of Science Research Centre.

REFERENCES

1. L.G. Van Uitert, *J. Chem. Phys*., **24**, 306 (1956).
2. E. Olsen and J. Thonstad, *J. Appl. Electrochem*., **29**, 293 (1999).
3. C.O. Augustion, D. Prabhakaran and L.K. Srinivasan, *J. Mater. Sci. Lett*., **12**, 383 (1993).
4. 4. A. Goldman, Handbook of Modern Ferromagnetic Materials, Springer Science + Business Media, New York (1999).
5. J. Smith and H.P.J.Wijn, Ferrites, John Wiley & Sons Publ., Netherlands (1959).
6. N.M. Deraz, *Ceram. Int*., **38**, 511 (2012).
7. N.M. Deraz and S. Shaban, *J. Anal. Appl. Pyrolysis*, **86**, 173 (2009).
8. M.K. Shobana, S. Sankar and V. Rajendran, *J. Alloys Comp*., **472**, 421 (2009).
9. A. Hussain, T. Abbas and S.B. Niazi, *Ceram. Int*., **39**, 1221 (2013).
10. Y. Köseoglu, I. Aldemir, F. Bayansal, S. Kahraman and H.A. Çetinkara, *Mater. Chem. Phys*., **139**, 789 (2013).
11. H. Yang, L. Zhao, X. Yang, L. Shen, L. Yu, W. Sun, Y. Yan, W. Wang and S. Feng, *J. Magn. Magn. Mater*., **271**, 230 (2004).
12. H.-F. Yu and S.-W. Yang, *J. Alloys Comp*., **394**, 286 (2005).
13. M. Airimioaei, C.E. Ciomaga, N. Apostolescu, L. Leontie, A.R. Iordan, L. Mitoseriu and M.N. Palamaru, *J. Alloy. Comp*., **509**, 8065 (2011).
14. B.D. Cullity, Elements of X-ray Diffraction; Addison-Wesly Publishing Co. Inc., Ch. 14 (1976)..
15. V.K. Sankaranarayanan and C. Sreekumar, *Curr. Appl. Phys*., **3**, 205 (2003).
16. S.L. Blank and J.A. Pask, *J. Am. Ceram. Soc*., **52**, 669 (1969).
17. A.M. Alper, High Temperature Oxides, Academic Press, New York (1970).
18. A. Azhari, M. Sharif Sh, F. Golestanifard and A. Saberi, *Mater. Chem. Phys*., **124**, 658 (2010).
19. R.M. Cornell and U. Schwertmann, The Iron Oxides: Structure, Properties, Reactions, Occurrence and Uses, VCH, New York (1996).
20. S. Sun, H. Zeng, D.B. Robinson, S. Raoux, P.M. Rice, S.X. Wang and G. Li, *J. Am. Chem. Soc*., **126**, 273 (2004).
21. Y. Köseoglu, *Ceram. Int*., **39**, 4221 (2013).
22. N.M. Deraz and A. Alarifi, *J. Anal. Appl. Pyrolysis*, **94**, 41 (2012).